Quantifying Glioblastoma Drug Response Dynamics Incorporating Treatment Sensitivity and Blood Brain Barrier Penetrance From Experimental Data

Susan Christine Massey[1], Javier C. Urcuyo[1], Bianca Maria Marin[2], Jann N. Sarkaria[2] and Kristin R. Swanson[1,3,4]*

[1] Precision Neurotherapeutics Innovation Program, Mayo Clinic, Phoenix, AZ, United States, [2] Department of Radiation Oncology, Mayo Clinic, Rochester, MN, United States, [3] Department of Neurological Surgery, Mayo Clinic, Phoenix, AZ, United States, [4] School of Mathematical and Statistical Sciences, Arizona State University, Tempe, AZ, United States

Many drugs investigated for the treatment of glioblastoma (GBM) have had disappointing clinical trial results. Efficacy of these agents is dependent on adequate delivery to sensitive tumor cell populations, which is limited by the blood-brain barrier (BBB). Additionally, tumor heterogeneity can lead to subpopulations of cells with different sensitivities to anti-cancer drugs, further impacting therapeutic efficacy. Thus, it may be important to evaluate the extent to which BBB limitations and heterogeneous sensitivity each contribute to a drug's failure. To address this challenge, we developed a minimal mathematical model to characterize these elements of overall drug response, informed by time-series bioluminescence imaging data from a treated patient-derived xenograft (PDX) experimental model. By fitting this mathematical model to a preliminary dataset in a series of nonlinear regression steps, we estimated parameter values for individual PDX subjects that correspond to the dynamics seen in experimental data. Using these estimates as a guide for parameter ranges, we ran model simulations and performed a parameter sensitivity analysis using Latin hypercube sampling and partial rank correlation coefficients. Results from this analysis combined with simulations suggest that BBB permeability may play a slightly greater role in therapeutic efficacy than relative drug sensitivity. Additionally, we discuss recommendations for future experiments based on insights gained from this model. Further research in this area will be vital for improving the development of effective new therapies for glioblastoma patients.

Keywords: glioblastoma, blood–brain barrier, drug sensitivity, epidermal growth factor receptor (EGFR), parameter estimation

1. INTRODUCTION

Glioblastoma (GBM) is an aggressive primary brain cancer that is notoriously difficult to treat due to its diffuse infiltration into surrounding normal-appearing brain (Giese et al., 2003). These diffusely invading GBM cells cannot be completely resected surgically (Baldock et al., 2014), and are difficult to target with radiation therapy while sparing normal brain (Corwin et al., 2013).

As a result, clinicians rely on chemotherapy to treat the full extent of the tumor. However, chemotherapeutic efficacy can be limited in two main ways: there may be insufficient delivery across the blood–brain barrier (BBB), and the tumor may not be uniformly sensitive to the agent.

The BBB acts to keep pathogens and many toxins out of the sensitive brain tissue. Angiogenesis in dense tumor regions induces disruption of the BBB, potentially allowing chemotherapeutic drugs to "leak" into these tumor regions. Current dogma in neuro-oncology holds this as being largely sufficient to treat the tumor, but GBM cells invade beyond these regions into tissue where the BBB remains rather intact (Van Tellingen et al., 2015). Further, tissue interstitial pressure and drug properties such as lipophilicity and polarity may influence the delivery of drugs across angiogenesis-induced BBB "leaks" (Ningaraj, 2006). Due to these factors, it remains unclear whether the delivery of BBB-impermeable antineoplastic agents reaches adequate concentrations throughout the tissue to provide the anticipated therapeutic effect.

Drug insensitivity (which includes, but is not limited to resistance) of tumor subpopulations is also a key suspect behind unsuccessful molecularly-targeted therapy results (Wen and Kesari, 2008; Ene and Holland, 2015). GBMs frequently present with gene mutations and/or amplification for a number of targets, such as epidermal growth factor receptor (EGFR). However, due to the spatial heterogeneity of GBM, these targets may have been identified for a subpopulation that is predominant in the dense tumor core, but less common in the invading portions of the tumor. There may also be activated compensatory signaling pathways in some cells or tumor regions that confer reduced responsiveness to the drug. Thus, while therapies already exist for molecular targets identified in GBM (Nagane et al., 1996; Brennan et al., 2013; Eskilsson et al., 2017; Reardon et al., 2017; van den Bent et al., 2017), a significant proportion of tumor may be less sensitive to these drugs, potentially explaining why they have failed in clinical trials (de Groot et al., 2008; De Witt Hamer, 2010; Reardon et al., 2010; AbbVie, 2019). However, it has been difficult to separate the possible insensitivity related causes of drug failure from that of inadequate delivery across the BBB and distribution throughout the tumor, since the majority of these drugs were not developed specifically for brain.

In order to explore both the contributions of inadequate delivery of therapy across the BBB and drug insensitivity, we developed a minimal mathematical model based on experimental data from preclinical subjects treated with an EGFR-targeted antibody drug conjugate (ADC). First, we describe model development based on this data, which consists of two tumor subpopulations with high vs. low sensitivity to the ADC therapy, and steps to estimate parameter regimes via data-fitting. Next, we explore the global model parameter sensitivity to understand how these parameters impact model outcomes. Finally, we run model simulations for the data-derived parameter regimes to assess the relative contributions of drug distribution and sensitivity, and discuss how it might be useful in assessing results

from future experiments comparing different tumor models or different drugs. Overall, our model suggests that the degree of drug exposure may be more impactful than the relative sensitivity to therapy between the tumor subpopulations. Thus, in order to improve treatment outcomes, it is critical to determine predictors of drug distribution in individual patients' tumors and surrounding brain tissue to ensure invading tumor cells are adequately exposed to the therapy.
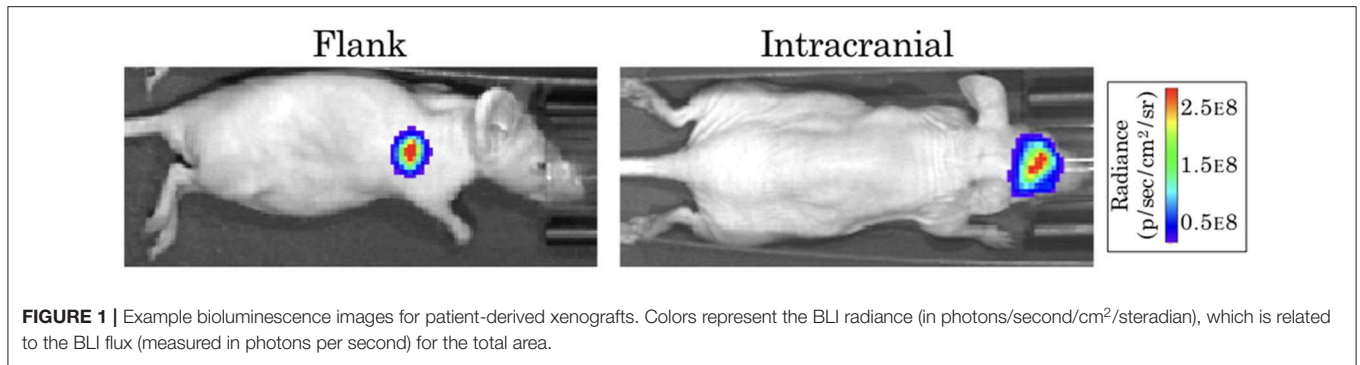
2. METHODS

Our ordinary differential equation (ODE) model of tumor growth and treatment response accounts for both variable treatment exposure and differential sensitivity to treatment by different tumor subpopulations. Development of this model was informed by experimental observations, which were also used to determine relevant parameter regimes for running simulations.

2.1. Experimental Data

The form of our model was based on experimental data from testing an EGFR-targeted antibody drug conjugate (ADC) in a patient-derived xenograft (PDX) model of GBM (Marin et al., 2018). These experiments were performed in full accordance with the guidelines of the Mayo Clinic Institutional Animal Care and Use Committee. The GBM12 PDX line used in this model is derived from a primary GBM in a male patient, and is EGFR amplified, MGMT methylated, and IDH1 and IDH2 wildtype. Full detail regarding this PDX line is available from the Mayo Clinic Brain Tumor Patient-Derived Xenograft National Resource (https://www.mayo.edu/research/labs/translational-neuro-oncology/mayo-clinic-brain-tumor-patient-derived-xenograft-national-resource/), where the line was developed and is maintained. These cells were implanted intracranially into 10 female athymic nude mice, and into the flank of 10 additional mice. After tumors were established, a subset of the surviving mice in each group was treated with either 10 mg/kg of a sham control antibody (Ab-095; four mice in each), or with 5 mg/kg of ABT-414 (an ADC also known as depatuxizumab mafodotin; five mice in each), administered via tail vein injection every 7 days. Tumor growth was monitored via bioluminescent imaging (BLI, **Figure 1**). Since BLI flux is *linearly* correlated with tumor cell number (Hartung et al., 2014), this provided us with a close approximation of tumor cell populations across time. Importantly, the data from PDX tumors grown in the flank and brain allowed us to compare treatment effect in tumors with and without BBB impediments to drug distribution.

2.2. Treatment Exposure and Sensitivity Model

Our model consists of three coupled ordinary differential equations describing the dynamics of both cell populations (H,

FIGURE 1 | Example bioluminescence images for patient-derived xenografts. Colors represent the BLI radiance (in photons/second/cm^2/steradian), which is related to the BLI flux (measured in photons per second) for the total area.

L) and the ADC (A):

$$\frac{dH}{dt} = \underbrace{\rho H}_{\text{proliferation}} - \underbrace{\gamma \mu_H A H}_{\text{drug-induced apoptosis}} \quad (1a)$$

$$\frac{dL}{dt} = \underbrace{\rho L}_{\text{proliferation}} - \underbrace{\gamma \mu_L A L}_{\text{drug-induced apoptosis}} \quad (1b)$$

$$\frac{dA}{dt} = \underbrace{\sum_{n=1}^{N} A_{\text{dose}}(n)\delta(t - 7n)}_{\text{drug dose given at time } t} - \underbrace{\lambda A}_{\text{drug decay}} \quad (1c)$$

where parameters and their definitions are outlined in **Table 1**, and their derivations can be found in section 2.3.

In the absence of the ADC, both highly sensitive (H) and less-sensitive (L) tumor populations grow exponentially, at proliferation rate ρ. However, the two populations differ in sensitivity to the ADC, A, which is captured by the drug-induced apoptosis rates μ_H and μ_L (for populations with high and low sensitivity, respectively). The terms for tumor cell death due to ADC are further modified by factor γ, which represents the proportion of cells exposed to ADC. We assume that the ADC is readily distributed to flank PDXs such that tumor cell exposure is high ($\gamma = 1$), but that the BBB limits this distribution for intracranial PDXs ($0 \leq \gamma \leq 1$). In order to capture the ADC dynamics, we let $A_{\text{dose}}(n)$ represent the nth dose, with doses administered every seven days, as noted by the dirac delta function $\delta(t - 7n)$. The ADC then decays at rate λ. These dynamics are schematized in **Figure 2**.

The model as described incorporates several assumptions that are useful to note explicitly. (1) While in theory there may be many groups of cells with varying levels of therapeutic sensitivity (some of which may even encapsulate resistant subpopulations), the model divides these into two main groups: those of relatively high therapeutic sensitivity and those with lower sensitivity to the therapy. (2) Any drug effect on proliferation rate is captured by the cell death rate parameter, as these effects are indistinguishable with the available data. (3) The effects of the tissue environment in the flank vs. the brain on tumor *growth* are encapsulated in environment-specific cellular proliferation rate parameter values (ρ_{flank} and ρ_{IC}, as described in section 2.3). (4) Relatedly, the cell death rate due to therapy for the sensitive tumor subpopulation,
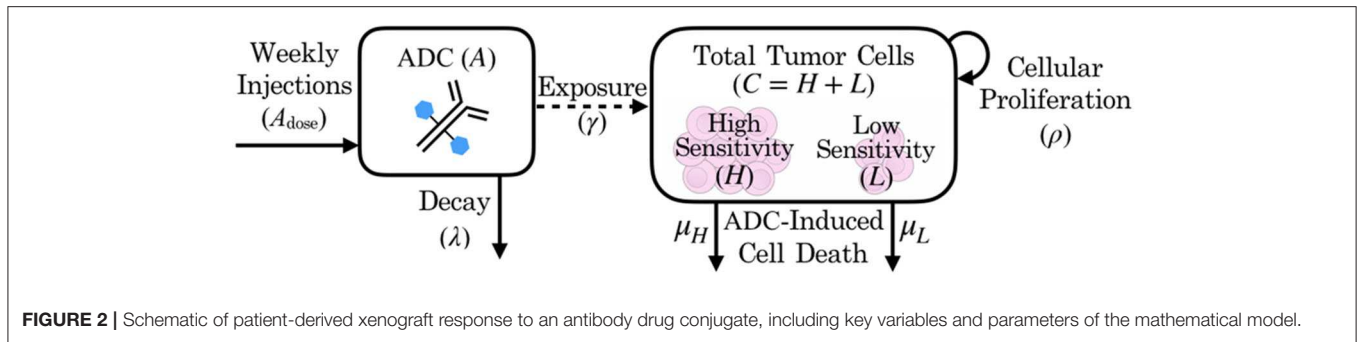
TABLE 1 | Model parameter definitions and values.

Symbol	Definition	Value range	Units
ρ	cellular proliferation rate	0.2–0.5	day^{-1}
μ_H	ADC-mediated high sensitivity cell kill rate	1–10	mg^{-1}day^{-1}
μ_L	ADC-mediated low sensitivity cell kill rate	$z\mu_H$	mg^{-1}day^{-1}
q	proportion of implanted cells with low sensitivity	0–1	unitless
z	relative sensitivity (μ_L/μ_H)	0–1	unitless
λ	rate of ADC decay	ln(2)/7	day^{-1}
γ	proportion of tumor exposed	0–1	unitless
A_{dose}	ADC given in a single dose	0.1	mg

Parameter value ranges were estimated through fitting the model to experimental data or parameters were confined to a value range by their theoretical meaning, except in the case of ADC parameters, as described in section 2.3.

μ_H, is assumed to be the same intracranially as in the flank setting, only modified by drug exposure after crossing the BBB in intracranial tumors. That is, the model assumes that the only environmental effect on *treatment* is its distribution. (5) ADC and tumor subpopulations are well-mixed. In reality there is likely spatial variation in both flank and intracranial sites due to the tumor microenvironment and different blood vessel densities in particular tumor regions, but in the absence of spatially–resolved data, we assume well-mixedness and use an ODE model.

This model can be solved analytically, as shown in **Appendix**. For simplification, at any given time t, $C(t)$ represents the total number of cells, calculated by the sum of high sensitivity $H(t)$ and low sensitivity $L(t)$ cells. This total cell number was used in section 2.3 for comparing with bioluminescence imaging data, which shows the total tumor cell population. The initial proportion of total implanted cells with low sensitivity is denoted by $q = L_0/C_0$. Similarly, the extent to which these cells L are less sensitive to the agent than the highly sensitive cells H is denoted by the relative sensitivity ratio $z = \mu_L/\mu_H$, which is bounded between 0 and 1 to ensure that μ_L is a fraction of μ_H in the regression-based parameterization in section 2.3. With these notational changes, we can then write the analytical solution (derived in **Appendix**) as

$$C(t) = C_0 e^{\rho t}\left(qe^{-\gamma\mu_H \int A(t)dt} + (1-q)e^{-\gamma z\mu_H \int A(t)dt}\right), \quad (2)$$

FIGURE 2 | Schematic of patient-derived xenograft response to an antibody drug conjugate, including key variables and parameters of the mathematical model.

where

$$\int A(t)dt = \sum_{n=1}^{N} 2^n A_{\text{dose}}(n) \frac{\left(e^{7n\lambda} - e^{\lambda t}\right)\theta(t - 7n)}{\lambda}. \quad (3)$$

Using this solution (2), the model can be parameterized through comparison of simulations to time-series BLI data.

2.3. Data-Based Parameter Estimation

Most model parameters were unknown, with the exception of ADC-specific parameters: the timing of dose administration and dose amounts $[A_{\text{dose}}(n)]$, as well as the half-life of the drug, which allowed us to solve for the drug decay rate (λ). Dose amounts were adjusted for the weight of each animal (5 mg/kg), so we applied the average initial animal weight of 20 g to obtain the constant ADC dose, $A_{\text{dose}} = 0.1$ mg used in simulations. All of the remaining model parameters were determined through several iterations of fitting the model via least squares regression to preliminary BLI data from an experiment. The various arms of the experiment included untreated and treated groups of subjects, as well as flank and intracranial tumor sites to separate out BBB influences. By fitting the model to these various subgroups, we were able to identify and estimate each of the parameters, as described below.

Step 1: Fit to untreated data to estimate growth rate, ρ. When fitting the model to untreated data, since the ADC is not injected ($A = 0$), the model's treatment components zero out and only an exponential growth function remains: $C(t) = C_0 e^{\rho t}$. Fitting this model function to untreated data via least squares regression with the `lsqcurvefit` function in MATLAB® (MATLAB Release 2018b, The MathWorks, Inc., Natick, Massachusetts, United States), we were able to obtain estimates of the tumor proliferation rate, ρ, and the number of viable implanted PDX cells, C_0 (**Figure 3**). (While a consistent number of cells are initially implanted for each subject, C_0 is in fact unique for each, as a variable number of cells die off, possibly due to an inability to establish themselves in the proper microenvironment for growth.) This yielded subject-specific values for ρ and C_0 (which were bound on the intervals $[0, \inf]$ and $[10^2, 10^{10}]$, respectively), and the mean ρ was recorded as the net proliferation rate for the cells of the particular PDX line used in the experiments grown in either the flank (ρ_{flank}) or intracranial (ρ_{IC}) setting. As noted in the model assumptions, these site–specific ρ parameter values from untreated tumors are

used to help to account for microenivironmental effects on PDX growth in the two different locations that are independent of the BBB.

Step 2: Fit to treated flank data to estimate μ_H, z, and q. Using the estimated net proliferation rate ρ_{flank} from the previous step, we proceed to fit the treated data in the flank. We assume the estimate of ρ_{flank} remains the same in the treated case as untreated, since the microenvironment remains similar and any differences should be encapsulated in the treatment effect term. Additionally, since the tumor was injected in the flank, there is no BBB effect to limit the proportion of tumor exposed to the ADC, such that the exposure parameter $\gamma = 1$. The initial condition C_0 is fit using the initial untreated time point and the passed mean ρ_{flank} value. Pairing these with other known parameters (see **Table 1**), the only remaining three unknown parameters to be fit to the data are the cell death rates due to drug, μ_H and μ_L, for the two cell populations and the proportion of implanted cells that have low sensitivity, q. Using the definition $z = \mu_L/\mu_H$ and the analytical solution of the model (2), we can then apply a nonlinear least squares regression (again using `lsqcurvefit`) to fit subject-specific parameters for parameters μ_H, z, and q (bound on the intervals $[1, 10]$, $[0, 1]$ and $[10^{-10}, 10^{-2}]$, respectively).

Step 3: Fit to treated intracranial data to estimate γ, z, and q. Proceeding to fit the data from treated intracranial tumors, we apply the same approach to estimate parameters as in the flank, this time assuming that the estimate of ρ_{IC} from the untreated setting remains the same for the treated intracranial tumors due to a similar microenvironment. Again we determine the initial condition C_0 by fitting the untreated model with the passed mean ρ_{IC} value to the initial untreated time point. Because we assume that the cell death rate due to ADC for the highly sensitive tumor subpopulation (μ_H) is the same intracranially as in the flank setting, we pass the average μ_H value determined in Step 2 and estimate parameter γ, the fraction of tumor exposed to therapy, in addition to parameters z and q.

At the conclusion of these steps (summarized in **Figure 3**), all unknown model parameters had net and individual estimates. Note that no more than three parameters were fitted with any experimentally-derived data set, in order to reduce the potential for overfitting. To examine this further, initial parameter guesses for `lsqcurvefit` were selected from within the value ranges listed in **Table 1**, and we had mostly consistent convergence using low, middle, and high values (see **Supplementary Material**). Additionally, as we show in the **Figure 3** plots with dash–dot
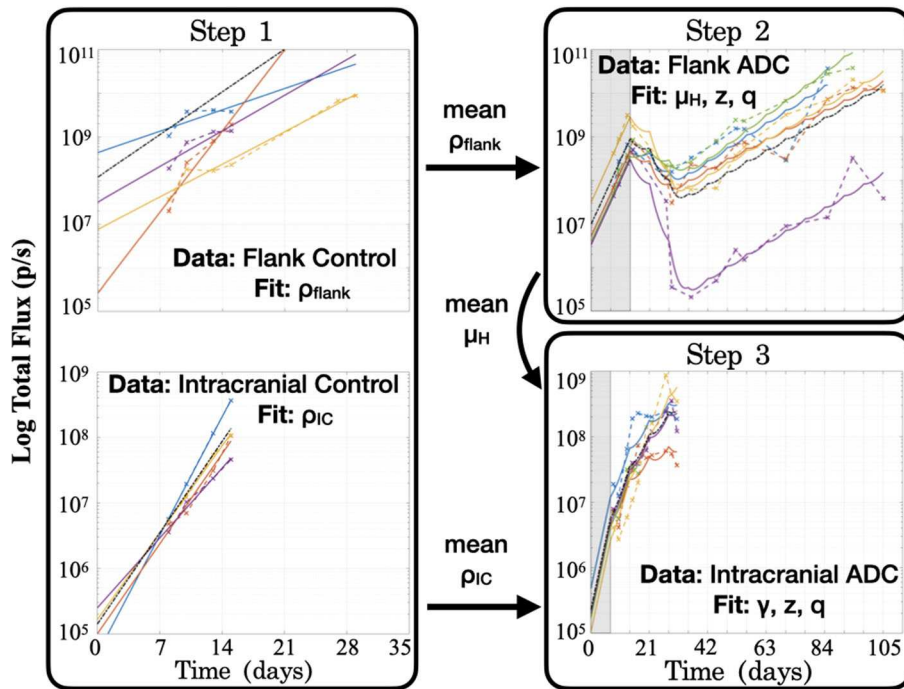
FIGURE 3 | Summary of the series of steps used to estimate model parameter values through fitting the model to different experimental data sets. **Step 1** consists of two separate fittings for the two different tumor locations, and the mean ρ values are passed for use in subsequent steps in the respective tumor sites, while the mean μ_H value from the flank found in **Step 2** is passed for use in **Step 3**. Shaded regions for Steps 2 and 3 indicate time prior to initiation of treatment with the ADC. Black dash–dot lines in each plot are simulations using the averaged fitted parameter values across all subjects within the group. It is worth noting that at each step, no more than three parameters are fitted to the data, in order to ensure identifiability and prevent overfitting.

lines, the simulations that result when using the averages of the fitted parameter values across all the subjects capture the dynamics of the data well. Thus, the averaged ρ_{flank}, ρ_{IC}, and μ_H values that we pass for later fitting steps correspond well with the group as a whole. Using these values then allowed us to run simulations in a reasonable range of parameter values, as well as to perform a model sensitivity analysis to understand how variability in these values affect model outcomes.
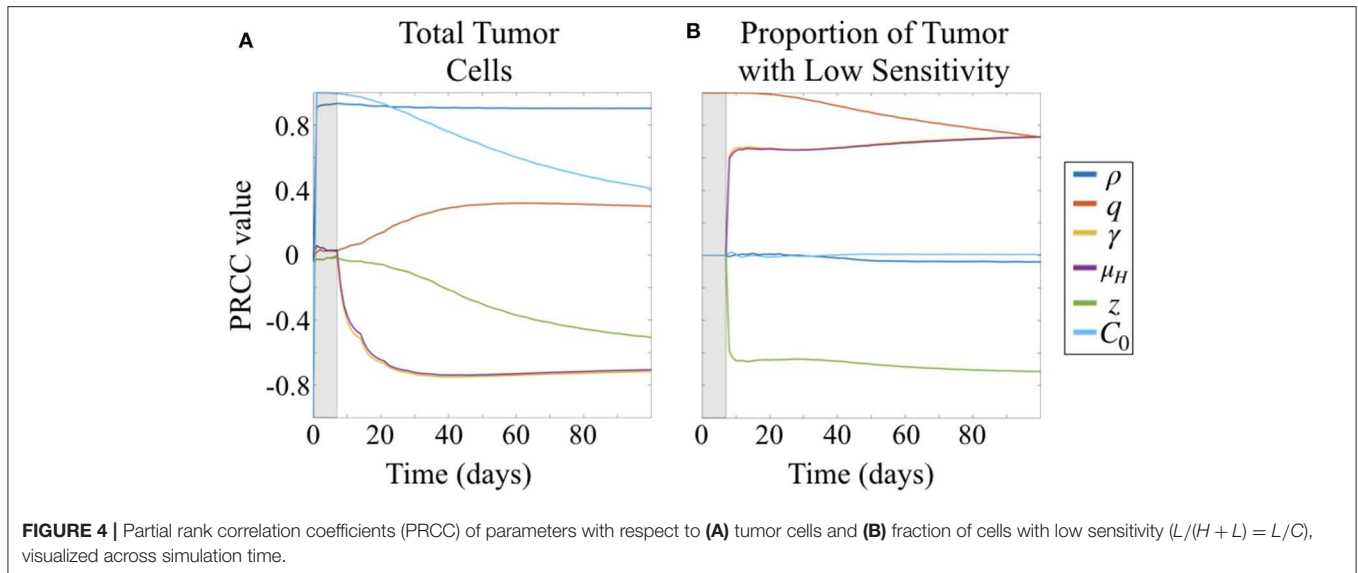
3. RESULTS

3.1. Parameter Sensitivity Analysis

Due to the uncertainty and variability in our parameter estimates, it was important to better characterize the effects of parameters on model results. To do this, we conducted a parameter sensitivity analysis via Latin hypercube sampling (LHS) and partial-rank correlation coefficients (PRCC) (McKay et al., 1979; Iman and Helton, 1988; Blower and Dowlatabadi, 1994). To perform the LHS analysis, we first drew 1,000 equiprobable samples for each unknown parameter, including the initial condition C_0, from a statistical distribution of values. These distributions were informed by our fits of the preliminary data when available; in the case of the unitless parameters, we assumed a uniform distribution on the interval $[0, 1]$. These samples were then randomly paired in a Latin hypercube scheme to run a series of 1,000 Monte Carlo simulations. Using these

simulation results, we then computed PRCCs between each parameter and two different model outcomes across all time points: the total number of tumor cells and the fraction of tumor that has low sensitivity (**Figure 4**). PRCC are computed using partial correlation applied to value ranks, as opposed to the actual values of the parameters and model outcome. Partial correlation helps control for effects due to other covariates, and ranks are used to evaluate the associative relationship between high and low values of parameters and the model outcomes, rather than the values themselves. Thus, the PRCC values at a given time point indicate how closely a high model outcome value relates to a high or low parameter value given at that time in the simulation. A PRCC close to 1 indicates a strong association between high parameter value and high model outcome value, and a PRCC close to -1 indicates a strong association between a low parameter value and a high model outcome value. For PRCC values between -0.5 and 0.5, the association is considered to be weak. Further details for about this method and the code files used are available on GitHub: https://github.com/scmassey/model-sensitivity-analysis.

3.1.1. Total Tumor Population Depends Most Strongly on Proliferation Rate, Followed by Treatment Response Parameters

At early time points, particularly before the initiation of therapy, the tumor population is strongly positively correlated with both

FIGURE 4 | Partial rank correlation coefficients (PRCC) of parameters with respect to **(A)** tumor cells and **(B)** fraction of cells with low sensitivity ($L/(H+L) = L/C$), visualized across simulation time.

the initial number of cells implanted, C_0 and proliferation rate ρ (**Figure 4A**). By 30 days, or after approximately three doses of therapy, the population remains strongly positively correlated with ρ but the effect of C_0 begins to wane. At the same time, drug sensitivity of the H cell population, μ_H, and exposure to drug, γ are strongly negatively correlated with total tumor cells. Relative sensitivity z, which determines the fraction of drug sensitivity in the L cell population, is also negatively correlated with total tumor, but less strongly, and only approaches a PRCC value of -0.5 after 100 days. This suggests that relative sensitivity z is less impactful than either the treatment response rate μ_H for the subpopulation with high ADC sensitivity or the degree of tumor exposure to ADC, γ.

Parameters γ and μ_H track together in the sensitivity analysis (overlapping lines in **Figure 4**). This is expected given our substitution $\mu_L = z\mu_H$, which results in the coefficient $-\gamma z \mu_H$ in the term describing drug induced apoptosis for the equation describing the L population (Equation 1b), mirroring that for the H population (Equation 1a), $-\gamma \mu_H$. Thus, sensitivity analysis is unable to compare the differential impacts of these two parameters, and highlights a potential parameter identifiability issue for our model. Since we had preliminary data in both the treated flank as well as the treated intracranial PDX settings, we were able to obtain parameter estimates for these by keeping $\gamma = 1$ in the flank setting, and assuming that μ_H is the same intracranially as in flank.

3.1.2. Less Sensitive Fraction of Tumor Driven by Initial Proportion of These Cells, Followed by Treatment Response Parameters

Prior to the initiation of therapy, only parameter q, the fraction of initially implanted cells that have low sensitivity, is correlated with the proportion of total tumor that has low sensitivity (**Figure 4B**). Once treatment is initialized, q remains highly positively correlated, and this correlation decreases slightly over time during the course of treatment.
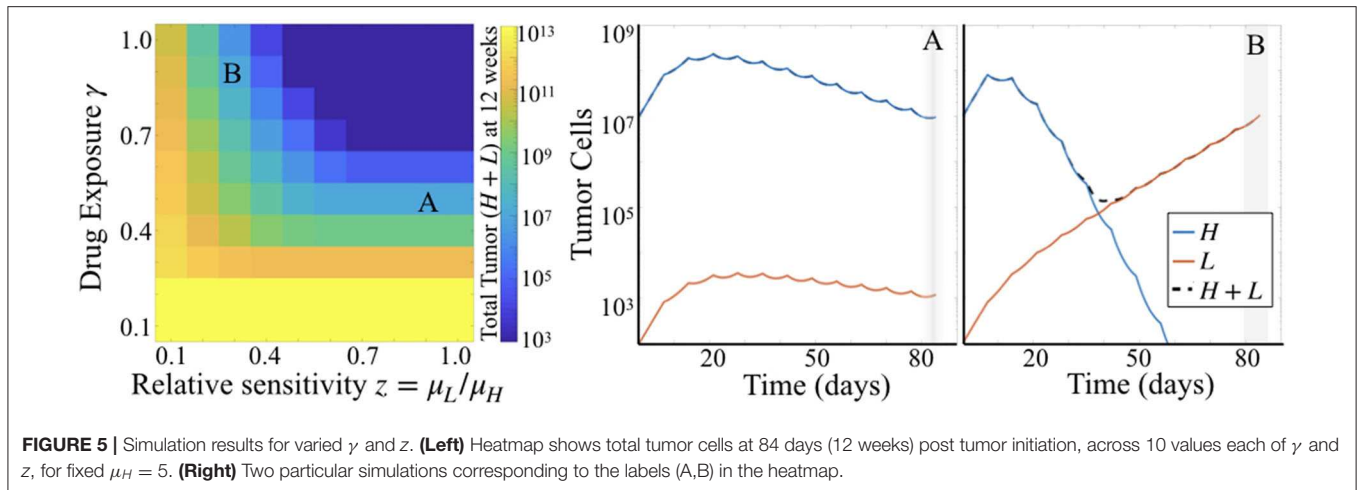
Three other parameters show correlation with the fraction of tumor that has lower sensitivity following initiation of therapy, all of which involve drug response. Parameters γ and μ_H, representing the degree of tumor exposure to ADC and the ADC-induced cell kill rate of cells with high sensitivity, respectively, are both positively correlated and track together, while parameter z, representing the relative treatment sensitivity between the cells with higher and lower sensitivity, is negatively correlated with the fraction of tumor that has low sensitivity. Further, the PRCC values do not vary over the time of the simulation after treatment is initiated and sustained. These correlations are consistent with expectations from the behavior of the system described by the model.

3.2. Simulation Results

To more fully explore the effect of parameters on model predicted outcomes, we ran simulations for varied values of the parameters relating to treatment response: γ, μ_H, and z (degree of ADC exposure, the ADC response rate in cells with high sensitivity, and the relative sensitivity between the two tumor subpopulations, respectively). Codes used to run simulations and plot the results may be found on GitHub: https://github.com/scmassey/treatment-exposure-sensitivity-model.

3.2.1. Treatment Exposure Impacts Tumor Burden More Than Relative Sensitivity

Comparing simulation results across a range of values for parameters γ and z while holding μ_H fixed, we see that γ plays a larger influence on total tumor cells than does z. That is, looking across rows of drug exposure values γ, we see that for relative sensitivity $z > 0.6$, there is no variation in total tumor burden. For lower levels of drug exposure, this is even more pronounced, as tumor burden is quite high regardless of the relative sensitivity. This is consistent with the parameter sensitivity results of section 3.1.1, but shows the impact of this dynamic in greater detail.

FIGURE 5 | Simulation results for varied γ and z. **(Left)** Heatmap shows total tumor cells at 84 days (12 weeks) post tumor initiation, across 10 values each of γ and z, for fixed $\mu_H = 5$. **(Right)** Two particular simulations corresponding to the labels (A,B) in the heatmap.

3.2.2. Different Subpopulation Proportions Can Yield Same Total Tumor Burden

Simulations also highlighted that there can be distinct differences in the dynamics of the two subpopulations of cells underlying predicted tumor burden (**Figure 5**). Looking at long time scales—in this case at 12 weeks or 84 days, the average survival time of the treated subjects—we observe the effect of an extended time of treatment in the simulations. Comparing two simulations with the same predicted tumor burden, we see that one simulation retains a large proportion of cells with high sensitivity (**Figure 5A**), while another is made up almost entirely of cells with low treatment sensitivity (**Figure 5B**). Thus, while the overall tumor may look similar at many points along its trajectory if sampled sparsely, one is about to be "uncontrolled" at later time points, while the other will stay relatively stable.

4. DISCUSSION

Failure of targeted therapies in glioblastoma can be attributed to many different causes, many of which are driven by various aspects of tumor heterogeneity. These include the potential mismatch of treatment to target beyond the center of the tumor and/or inadequate delivery of therapy to these cells invading outlying brain parenchyma. Often these have been investigated separately, focusing either on sensitivity (through optimizing targets or overcoming resistance) (Cloughesy et al., 2014), or engineering approaches for enhancing drug delivery (Liu et al., 2010; Van Tellingen et al., 2015). Infrequently, elements of both are combined (Stein et al., 2018), but even in those cases the relative impact of these upon treatment outcomes has not been compared. Thus, we created our Treatment Exposure and Sensitivity model describing tumor growth and treatment response incorporating both exposure and differential sensitivity to therapy, based on experimental data, to investigate the relationship between them. Through parameter sensitivity analysis and simulation, we found that both can contribute in similar ways, but exposure may have a greater impact overall. In particular, for simulated tumors that were given

the same treatment responsiveness for the highly sensitive population, therapeutic exposure impacts tumor burden more than the relative sensitivity between the two tumor populations. Sensitivity analysis also revealed that parameter ρ is the strongest positive influence on total cell population, as expected, and distinguished between the effect of reduced therapeutic sensitivity (z) and exposure to therapy (γ) in reducing the total tumor population. Not only is there a difference in the magnitude of correlation between parameters γ and z with total tumor burden, there is also a difference in the temporal dynamics of the change in these correlations over time. The correlation coefficients between parameters and the fraction of the tumor with lower treatment sensitivity, however, is quite stable over time.

4.1. Limitations

Our model is relatively minimal by design, as the amount of available data constrains the number of model parameters we can fit. Thus, this model does not compare potential sources of differential treatment sensitivity (such as various mechanisms of resistance). Although tumor heterogeneity may actually provide for many populations with varying levels of sensitivity to therapy, as described in section 2.2 we assumed that these cluster toward more or less sensitive, reducing them to two. Larger data sets generated by similar studies in the future may support including more populations and additional mechanistic differences or interactions between them. Related to this, we were also limited in distinguishing BBB impacts from other microenvironmental effects when comparing data from tumors grown in the flank vs. the intracranial setting beyond the proliferation rate, ρ. For example, microenvironmental effects, such as vascular density, likely create regions of differential drug exposure (as well as regions of different tumor subpopulations). Experiments generating larger data sets and greater spatial detail would facilitate adding these features in future modeling efforts. Finally, while our present analysis of the model enables us to understand the overall dynamics between the parameters, we are not able to conclude anything with respect to efficacy of this particular drug among patients due to the use of a single PDX line. As we discuss

below, however, by using the parameter fitting method presented to estimate drug sensitivity and exposure across multiple PDX lines in future studies, it may be possible to gain insight in these factors across patients with this heterogeneous disease.

4.2. Model Recommendations for Future Experiments

Parameter sensitivity analysis of the model highlighted the necessity of having the flank and intracranial treatment groups for practical identifiability in obtaining estimates for therapeutic sensitivity (μ_H) and exposure (γ). This "tradeoff" between γ and μ_H was also observed in simulations and is expected given our model formulation. However, the emergence of this dynamic in the creation and parameter estimation of our model underscores that this relationship should be carefully considered in the design of experimental studies for new glioma therapies. Sensitivity analysis revealed that correlation coefficients between parameters and total tumor burden change most dramatically at earlier time points, and after approximately 50 days, change relatively little. This suggests that experiments conducted to examine the relationship between exposure and sensitivity to therapy should focus on collecting time course data more densely for the first 7 weeks as compared to longer times. As shown by simulations, there can be several parameterizations that fit tumor burden data at any single time which correspond to different proportions of cells with high and low sensitivity to treatment. Thus, time series data is essential for detecting differences in these and the contributions of the BBB (parameter γ) and relative sensitivity (z).

Because our Treatment Exposure and Sensitivity model is minimal and reduces mechanisms down to a few key parameters, it has great utility for fitting experimental data to estimate these parameters for individuals. Having these individual parameterizations is key to understanding the extent to which drug exposure and resistance each contributed to variations in outcome. In particular, quantifying drug sensitivity and exposure parameters for individual subjects within and between groups with additional therapies and PDX lines (better capturing interpatient, as well as intrapatient,

heterogeneity) may be a promising avenue for future research. This will provide further insights for developing novel approaches to therapy optimization—including delivery—for individual patients.

DATA AVAILABILITY STATEMENT

All datasets generated for this study are included in the article/**Supplementary Material**.

ETHICS STATEMENT

The animal study was reviewed and approved by Mayo Clinic Institutional Animal Care and Use Committee.

AUTHOR CONTRIBUTIONS

FUNDING

ACKNOWLEDGMENTS

SUPPLEMENTARY MATERIAL

The Supplementary Material for this article can be found online at: https://www.frontiersin.org/articles/10.3389/fphys.2020.00830/full#supplementary-material

REFERENCES

AbbVie (2019). *Abbvie Provides Update on Depatuxizumab Mafodotin (depatux-m), An Investigational Medicine for Newly Diagnosed Glioblastoma, an Aggressive Form of Brain Cancer [Press Release].* Available online at: https://news.abbvie.com/news/press-releases/abbvie-provides-update-on-depatuxizumab-mafodotin-depatux-m-an-investigational-medicine-for-newly-diagnosed-glioblastoma-an-aggressive-form-brain-cancer.htm (accessed September 3, 2019).

Baldock, A. L., Ahn, S., Rockne, R., Johnston, S., Neal, M., Corwin, D., et al. (2014). Patient-specific metrics of invasiveness reveal significant prognostic benefit of resection in a predictable subset of gliomas. *PLoS ONE* 9:e99057. doi: 10.1371/journal.pone.0099057

Blower, S. M., and Dowlatabadi, H. (1994). Sensitivity and uncertainty analysis of complex models of disease transmission: an HIV model, as an example. *Int. Stat. Rev.* 229–243. doi: 10.2307/1403510

Brennan, C. W., Verhaak, R. G., McKenna, A., Campos, B., Noushmehr, H., Salama, S. R., et al. (2013). The somatic genomic landscape of glioblastoma. *Cell* 155, 462–477. doi: 10.1016/j.cell.2013.09.034

Cloughesy, T. F., Cavenee, W. K., and Mischel, P. S. (2014). Glioblastoma: from molecular pathology to targeted treatment. *Annu. Rev. Pathol.* 9, 1–25. doi: 10.1146/annurev-pathol-011110-130324

Corwin, D., Holdsworth, C., Rockne, R. C., Trister, A. D., Mrugala, M. M., Rockhill, J. K., et al. (2013). Toward patient-specific, biologically optimized radiation therapy plans for the treatment of glioblastoma. *PLoS ONE* 8:e79115. doi: 10.1371/journal.pone.0079115

de Groot, J. F., Gilbert, M., Aldape, K., Hess, K. R., Hanna, T., Ictech, S., et al. (2008). Phase II study of carboplatin and erlotinib (tarceva, osi-774) in patients with recurrent glioblastoma. *J. Neuro-Oncol.* 90, 89–97. doi: 10.1007/s11060-008-9637-y

De Witt Hamer, P. C. (2010). Small molecule kinase inhibitors in glioblastoma: a systematic review of clinical studies. *Neuro-oncology* 12, 304–316. doi: 10.1093/neuonc/nop068

Ene, C. I., and Holland, E. C. (2015). Personalized medicine for gliomas. *Surg. Neurol. Int.* 6(Suppl. 1):S89. doi: 10.4103/2152-7806.151351

Eskilsson, E., Røsland, G. V., Solecki, G., Wang, Q., Harter, P. N., Graziani, G., et al. (2017). EGFR heterogeneity and implications for therapeutic intervention in glioblastoma. *Neuro-Oncology* 20, 743–752. doi: 10.1093/neuonc/nox191

Giese, A., Bjerkvig, R., Berens, M., and Westphal, M. (2003). Cost of migration: invasion of malignant gliomas and implications for treatment. *J. Clin. Oncol.* 21, 1624–1636. doi: 10.1200/JCO.2003.05.063

Hartung, N., Mollard, S., Barbolosi, D., Benabdallah, A., Chapuisat, G., Henry, G., et al. (2014). Mathematical modeling of tumor growth and metastatic spreading: validation in tumor-bearing mice. *Cancer Res.* 74, 6397–6407. doi: 10.1158/0008-5472.CAN-14-0721

Iman, R. L., and Helton, J. C. (1988). An investigation of uncertainty and sensitivity analysis techniques for computer models. *Risk Anal.* 8, 71–90. doi: 10.1111/j.1539-6924.1988.tb01155.x

Liu, H.-L., Hua, M.-Y., Chen, P.-Y., Chu, P.-C., Pan, C.-H., Yang, H.-W., et al. (2010). Blood-brain barrier disruption with focused ultrasound enhances delivery of chemotherapeutic drugs for glioblastoma treatment. *Radiology* 255, 415–425. doi: 10.1148/radiol.10090699

Marin, B., Mladek, A., Burgenske, D., He, L., Hu, Z., Bakken, K., et al. (2018). Ddis-01. the antibody-drug conjugate ABT-414 demonstrates single-agent anti-cancer activity across a panel of GBM patient-derived xenografts. *Neuro-Oncology* 20(Suppl. 6):vi69. doi: 10.1093/neuonc/noy148.280

Massey, S. C., Urcuyo, J. C., Marin, B. M., Sarkaria, J., and Swanson, K. R. (2019). Quantifying glioblastoma drug response dynamics incorporating resistance and blood brain barrier penetrance from experimental data. *bioRxiv.* doi: 10.1101/822585

McKay, M. D., Beckman, R. J., and Conover, W. J. (1979). Comparison of three methods for selecting values of input variables in the analysis of output from a computer code. *Technometrics* 21, 239–245. doi: 10.1080/00401706.1979.10489755

Nagane, M., Coufal, F., Lin, H., Bögler, O., Cavenee, W. K., and Huang, H.-J. (1996). A common mutant epidermal growth factor receptor confers enhanced tumorigenicity on human glioblastoma cells by increasing proliferation and reducing apoptosis. *Cancer Res.* 56, 5079–5086.

Ningaraj, N. S. (2006). Drug delivery to brain tumours: challenges and progress. *Expert Opin. Drug Deliv.* 3, 499–509. doi: 10.1517/17425247.3.4.499

Reardon, D. A., Desjardins, A., Vredenburgh, J. J., Gururangan, S., Friedman, A. H., Herndon, J. E., et al. (2010). Phase 2 trial of erlotinib plus sirolimus in adults with recurrent glioblastoma. *J. Neuro-Oncol.* 96, 219–230. doi: 10.1007/s11060-009-9950-0

Reardon, D. A., Lassman, A. B., van den Bent, M., Kumthekar, P., Merrell, R., Scott, A. M., et al. (2017). Efficacy and safety results of abt-414 in combination with radiation and temozolomide in newly diagnosed glioblastoma. *Neuro-Oncology* 19, 965–975. doi: 10.1093/neuonc/now257

Stein, S., Zhao, R., Haeno, H., Vivanco, I., and Michor, F. (2018). Mathematical modeling identifies optimum lapatinib dosing schedules for the treatment of glioblastoma patients. *PLoS Comput. Biol.* 14:e1005924. doi: 10.1371/journal.pcbi.1005924

van den Bent, M., Gan, H. K., Lassman, A. B., Kumthekar, P., Merrell, R., Butowski, N., et al. (2017). Efficacy of depatuxizumab mafodotin (abt-414) monotherapy in patients with EGFR-amplified, recurrent glioblastoma: results from a multi-center, international study. *Cancer Chemother. Pharmacol.* 80, 1209–1217. doi: 10.1007/s00280-017-3451-1

Van Tellingen, O., Yetkin-Arik, B., De Gooijer, M., Wesseling, P., Wurdinger, T., and De Vries, H. (2015). Overcoming the blood-brain tumor barrier for effective glioblastoma treatment. *Drug Resist. Updates* 19, 1–12. doi: 10.1016/j.drup.2015.02.002

Wen, P. Y., and Kesari, S. (2008). Malignant gliomas in adults. *New Engl. J. Med.* 359, 492–507. doi: 10.1056/NEJMra0708126